GSA Data Repository 2018185

Wild et al., 2018, Early stages of bacterial community adaptation to silicate aging: Geology, https://doi.org/10.1130/G40283.1.

ITEM DR 1. DETAILED METHODS

DR 1.1. Fluid collection at the Strengbach catchment

The Strengbach catchment is located in Aubure, France. Soil solution was collected in a beech plot located in the catchment (48°12’41.04"N; 7°11’45.66"E) with a polytetrafluoroethylene (PTFE) lysimeter plate located at 10 cm depth, in the A horizon of the soil profile. A polyethylene (PE) bag (Coplicel Willinger, Strasbourg, France) was placed at the output of the lysimetric system, protected by a sealed plastic barrel located in a ~1 m deep pit dug in the beech plot. About 30 L of soil solution were collected over 56 days (31/03/2015 to 26/05/2015). The bag was then isolated from the fluid input and stored *in situ* over a stabilization period of 100 days (26/05/2015 to 15/09/2015) that aimed at reaching a stable and homogeneous solution. Over the period extending from the sampling time to the end of the stabilization period, fluid temperature as well as temperature within the soil profile were regularly measured and attained a mean value of $T_{in\ situ}$ = 12.5 ± 3 °C. The solution was then transferred to the lab and stored for several days in the dark at $T = T_{in\ situ}$ prior to the beginning of the experiments.

DR 1.2 Mineral preparation and ageing

Experiments were conducted on olivine and labradorite. Olivine minerals used in this study consist in cm-sized translucent, bottle-green crystals of gem quality purchased from Wards Natural Science, with an average composition of $(Mg_{0.9}Fe_{0.1})_2SiO_4$. Labradorite

samples are translucent greyish cm-sized crystals containing Fe-rich inclusion, purchased from Mawingu Gems, with an average composition of $Si_{2.49}Al_{1.49}K_{0.02}Ca_{0.52}Na_{0.45}O_8$.

For both minerals, 200 g of cm-sized chunks were washed with MilliQ water and crushed with a hydraulic press. Collected powders were sieved to obtain a grain size fraction between 160 and 315 µm. Residual fine particles were then discarded by suspension into five successive MilliQ water baths followed by 5 min sonication steps in ethanol, until the supernatant remained clear. Powders were eventually rinsed with ethanol and dried in an oven at 30°C. The specific surface area (SSA) measured using the Brunauer-Emmet-Teller (BET) method was 0.051 $m^2.g^{-1}$ for the labradorite powder, and 0.058 $m^2.g^{-1}$ for the olivine powder, respectively.

Subsamples of the prepared powders were then reacted under conditions inducing their controlled ageing, namely T = 80°C, pH = 3.7 for olivine (Daval et al., 2011) and T = 80°C, pH = 3.0 for labradorite (Wild et al., 2016). Reacting solutions were saturated with respect to amorphous silica at 80°C in order to stabilize the amorphous surface layers. For both minerals, aged powders were obtained by introducing 4 g of powder into 60 ml flow-through reactors. The corresponding solutions were prepared from milliQ water, sodium metasilicate, nonahydrate (Sigma Aldrich®, >98%) and concentrated HCl (37%, ACS reagent), and were circulated at a flow rate of 1 $ml.min^{-1}$ for 20 days. Aged powders were recovered, briefly rinsed with milliQ water and ethanol, and dried in an oven at 30°C.

DR 1.3 Mounting flow-through set-ups in sterile conditions

All elements of the experimental set-ups that were to contact either the environmental fluid or the reacting powders—including 60 ml PTFE flow-through reactors, tubing, connectors, seals, stirring stands or magnetic bars—were autoclaved at 125°C, 20 psi for 15

min. Powders were washed for 10 minutes in sterile PTFE vessels with two successive baths of 0.2 µm filtered absolute ethanol, dried for >60 min under sterile laminar flow and exposed to ultraviolet radiation for 20 min. Weighed amounts of dried powders were rinsed and introduced into labelled reactors and all elements were connected under sterile flow. Once mounted, the entire airtight set-up was moved into the refrigeration device. A schematic description of the experimental set-up can be found in Figure DR 2.2.

DR 1.4 Experimental set-up

About half of the environmental fluid (~15 L) was sampled from the main container and filtered at 0.22 µm with sterile polyvinylidene fluoride (PVDF) membranes (Durapore®) under sterile laminar flow in order to withdraw most of the biotic content from the solution. The removal of bacteria by the filtration was assessed by epifluorescence microscopy (see Figure DR 2.8). Filtered and non-filtered environmental fluids were transferred into clean low-density polyethylene (LDPE) cubitainers, which were previously rinsed several times with 0.22 µm-filtered ethanol, dried under a sterile flow cabinet and rinsed with the appropriate input solution (either raw or sterilized).

The fluids were then circulated into a sterile flow-through set-up (see section DR 1.3) containing labradorite or olivine powders, either pristine or aged. Flow rate was set to 0.005 ± 0.002 $ml.min^{-1}$ for labradorite experiments and 0.03 ± 0.01 $ml.min^{-1}$ for olivine experiments. These values were calculated so as to match the optimal trade-off between cation detectability (signal/background maximization, which requires low flow rates) and maintenance of constant physicochemical parameters (in terms of pH or undersaturation with respect to dissolving and secondary phases, which require high flow rates). The whole set-up was maintained in the dark at 12 °C during the experiment. Duplicate reactors were operated in

parallel for each experiment. Note however that for the biotic experiment conducted on fresh labradorite powders, the fall of the stirrer at the beginning of the experiment caused grinding of the powder, yielding unexpectedly enhanced elemental release into solution (Table DR 2.2) and increase of the pH (Fig. DR 2.3). This duplicate experiment was therefore not taken into account for the analyses of the results.

DR 1.5 Monitoring of physicochemical parameters

Experiments were continuously sampled with sterile polypropylene (PP) Falcon® tubes placed at the output of the flow-through system. Cation concentrations were determined by ICP-AES measurements performed on a Thermo ICAP 6000 Series. The dissolution rate was calculated following:

$$R(X) = \frac{v * \Delta X}{m * S * \eta_X} \quad (1)$$

where v is the flow rate in $l.s^{-1}$, ΔX is the amount of element X released to the solution by the dissolution process, calculated as the difference between background and total output concentrations in $mol.l^{-1}$, m is the mass of mineral powder introduced inside the reactor in g, S is the Kr BET specific surface area of the pristine powder in $m^2.g^{-1}$, and η_X the stoichiometric coefficient of element X in the bulk mineral. Element X used to calculate rates displayed in Figure 1 were Mg and Ca for olivine and labradorite, respectively. Note that the use of the BET SSA of pristine powders as a proxy for the surface area of their passivated counterparts likely underestimates the actual surface area of the passivated powders, since the formation of passivating layers usually leads to the development of roughness, which that increases the actual SSA. As a consequence, the dissolution rates reported for passivated materials should be considered as an upper bound, and the estimated gap between passivated and non-passivated powders should be viewed as a minimal value.

Background concentrations used in the calculation of ΔX for olivine were estimated from the regular measurement of samples from the input solution. Since flow rates for labradorite were very low ($v = 5 \pm 2 \times 10^{-3}$ ml.min^{-1}), the background concentration estimated at the outlet of the reactor cannot be considered similar to the background concentration measured at the inlet of the reactor. In fact, the outlet concentration depends on the residence time of the fluid in the reactor. As a consequence, this "reservoir effect" of the system was taken into account. Applying a mass balance on the amount of tracer element issued from the input solution yields the following differential equation:

$$V.\frac{d(X_{out})}{dt}(t) = v((X_{in}(t)) - X_{out}(t)) \quad (2)$$

where V represents the volume of the reactor in l, t is the elapsed time of the experiment in s, and X_{in} and X_{out}, the concentrations in tracer element X measured at the inlet and estimated at the outlet of the reactor, respectively. A continuous function of time $X_{in}(t)$ was determined by fitting 6 input data points from ICP-AES measurements using a second order polynomial function (green line in Fig. DR 1.5). This was used to determine X_{out} at the desired time steps by solving numerically equation (2) using Matlab® software (blue line in Fig. DR 1.5). Note that such a treatment was not necessary for experiments conducted on olivine powders, since the high flow rate used for these experiments resulted in a negligible residence time of the solution in the reactors, so that the approximation $X_{in}(t) \approx X_{out}(t)$ is reasonable.

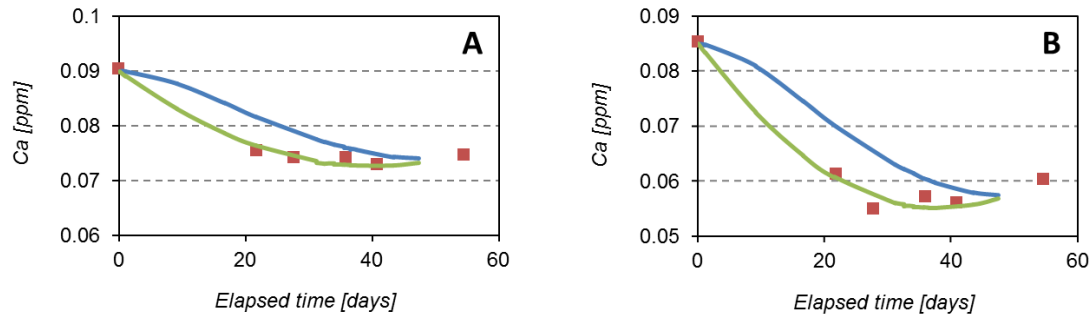

Fig. DR 1.5: Comparison between measured (red symbols), input (green line) and simulated output (blue line) Ca concentration evolution over time for filtrated (A) and non-filtrated (B) input fluids.

The capabilities of our analytical set-up with respect to the soil solution were assessed by measuring elemental concentrations in samples of environmental solution spiked with a known amount of tracer (Ca and Mg) ranging from 8.3 to 1950.0 ppb. The error on measurement (ε_X) was then determined as:

$$\varepsilon_X = \frac{\sqrt{(X_M - X_T)^2}}{(X_T)^2} \tag{3}$$

where X_M stands for the measured value and X_T for the true value as determined by weighing (weighing precision: ± 0.001 g over 10 g total) the spiked amount of ICP-AES standard (Inorganic Ventures, Christiansburg, VA).

The precision limit was estimated from a 15 % threshold (ε_X^{max}= 0.15) to be around 8 ppb for both Mg and Ca. This falls within the same order of magnitude as the limit of detection (LOD) (1.8 ppb for Ca and 8.7 ppb for Mg) and limit of quantification (LOQ) (10.7 ppb for Ca and 29.1 ppb for Mg) determined on the basis of 21 blank measurements performed during the same analysis. The analytical error was determined as the mean value over the concentration range measured in the experiment, yielding errors of 6.5 % for olivine concentrations and 8.9 % for labradorite. Since weighing was performed with a minimum precision of ± 0.05 %, and time with ± 0.05 % precision, errors on both the v and m terms in

equation (1) were negligible compared to the error on concentrations. No error could be estimated individually for each sample regarding Kr BET specific surface area; however, since all compared samples were randomly sourced from the same homogeneous stock, this systematic error was considered negligible. Therefore, errors reported for weathering rates in Figure 1 of the main text correspond to errors on tracer concentrations as estimated above.

Some samples were used for off-line pH measurements, performed with a Titrando 905 apparatus, coupled with an Aquatrode Plus® glass electrode and Tiamo 2.3 software (Metrohm, Herisau, Switzerland). Dissolved oxygen concentration in the input fluid was verified to be > 4 ppm at the end of the experiment with a dissolved oxygen sensor (HI 9828, Hanna Instruments, Tanneries, France).

Flow rate was independently measured from successive weighing of sampling tubes before and after each sampling.

DR 1.6 DNA extraction

Total DNA was extracted from filters and mineral powders with PowerWater® and PowerSoil® DNA Isolation Kits (MO BIO, Carlsbad, CA, USA) following manufacturer's instructions. In order to capture the complete genomic signature of the mineralosphere, the latter extraction kit includes a specific vortexing step aimed at cell detachment from solid surfaces and cell lysis by randomly shaking minerals with ceramic beads in the presence of disruption agents and was used on wet mineral powders. Concentrations of DNA were determined using the Qubit® Fluorometer and the Qubit® dsDNA HS Assay Kit (Invitrogen, Carlsbad, CA, USA).

DR 1.7 Illumina's MiSeq two-step sequencing

Sequencing was performed at Research and Testing Laboratory (Lubbock, TX, USA) using Illumina MiSeq technique. The 16S rRNA gene spanning the hypervariable region V4 was amplified in a two-step process.

The 16S bacterial barcoded primers 515F and 806R were used to amplify the 16S rRNA gene spanning the hypervariable region V4 on an Illumina MiSeq platform 2500.The forward primer was constructed with the Illumina i5 sequencing primer (5′-TCGTCGGCAGCGTCAGATGTGTATAAGAGACAG-3′) and the universal bacterial 515F (5′-GTGCCAGCMGCCGCGGTAA-3′) primer (Walters et al., 2011). The reverse primer was constructed with the Illumina i7 sequencing primer (5′-GTCTCGTGGGCTCGGAGATGTGTATAAGAGACAG-3′), and the bacterial "universal" 806R primer (5′-GGACTACHVGGGTWTCTAAT-3′). Sequences were generated by PCR in 25 µl reactions with the Qiagen HotStar Taq master mix (Qiagen Inc, Valencia, California), 1 µl of each 5 µM primer and 1 µl of template. Reactions were performed on ABI Veriti thermocyclers (Applied Biosytems, Carlsbad, California) under the following thermal profile: 95°C for 5 min, then 25 cycles of 94°C for 30 sec, 54°C for 40 sec, 72°C for 1 min, followed by one cycle of 72°C for 10 min and 4°C hold.

Products from the first stage amplification were added to a second PCR. Primers for the second PCR were designed based on the Illumina Nextera PCR primers as follows: Forward -AATGATACGGCGACCACCGAGATCTACAC[i5index]TCGTCGGCAGCGT and Reverse -CAAGCAGAAGACGGCATACGAGAT[i7index]GTCTCGTGGGCTCGG. The second stage amplification was run in the same conditions as in the first stage except for 10 cycles. Amplification products were visualized using eGels (Life Technologies, Grand Island, New York). Products were pooled equimolar and each pool was size-selected in two rounds using

Agencourt AMPure XP (BeckmanCoulter, Indianapolis, Indiana) in a 0.7 ratio for both rounds. Size-selected pools were quantified using the Qubit 2.0 fluorometer (Life Technologies) and loaded on an Illumina MiSeq (Illumina, Inc. San Diego, California) 2 × 300 flow cell at 10 pM.

DR 1.8 Processing of Illumina's MiSeq data

Denoising, chimera checking, generation of operational taxonomic units (OTUs) and taxonomic classification were performed using the custom-scripted bioinformatics pipeline of the Research and Testing Laboratory. Briefly, denoising and OTU generation were accomplished after conversion into FASTA formatted sequences and quality files using USEARCH (Edgar, 2010) and UPARSE OTU for OTU selection (Edgar, 2013). Chimera checking was performed using UCHIME algorithms executed in *de novo* mode (Edgar et al., 2011). Sequences were clustered into OTUs at different levels of sequence identity using the UPARSE algorithm. The centroid sequence from each cluster was then run against either the USEARCH global alignment algorithm or the RDP Classifier against a highly curated database compiled by Research and Testing Laboratory and originating from NCBI (http://nbci.nlm.nih.gov). Based upon sequence identity percentage derived from BLASTn, sequences with identity scores to known or well-characterized 16S sequences >97% identity (<3% divergence) were resolved at the species level, >95% to 97% at the genus level, >90% to 95% at the family level, >80% to 90% at the order level, >80 to 85% at the class level, and between 77% – 80% at the phylum level. Any match below this level of identity was not used in taxonomical analysis. Obtained matrices of taxonomic data were used for further statistical analysis, except for calculation of diversity and richness indices.

DR 1.9 Bacterial diversity and composition analyses

The Illumina MiSeq sequence datasets were re-analyzed using MOTHUR version 1.36.1 (http://www.mothur.org) starting from denoised and chimera checked sequences, aligned, and clustered to define OTUs at 97% sequence identity. A subsample of sequences was then randomly selected to obtain equally sized datasets according to the standard operating procedure (Schloss et al., 2009). Resulting datasets were used for calculation of diversity indices and for rarefaction analyses. Shannon's diversity index (H') was calculated as $H' = -\sum p_i \ln p_i$ and Inverse-Simpson's diversity index (I) was calculated as $I = 1/D$ with $D = \sum p_i^2$, where p_i is the relative abundance of species i. Chao1 richness estimate was calculated as $S_{chao1} = S_{obs} + {f_1^2}/{2 \times f_2}$, where S_{obs} is total number of OTUs in a sample, f_1 is the number of OTUs with only one sequence (i.e. "singletons") and f_2 the number of OTUs with only two sequences (i.e. "doubletons").

To visualize ecological gradients underlying bacterial community structures across our samples, principal coordinate analysis (PCoA) based on Bray-Curtis dissimilarities were performed in R with the vegdist function of the vegan package and the cmdscale function from the stats package. The relationship between community profiles of samples and the species variables was investigated by *a posteriori* projection of the variables as weighted average of their contribution to the samples onto the PCoA biplot. For each gradient represented by a PCoA axis, departure of a species variable from the central value (0) emphasizes an overweighting of this species in the samples positioned in the corresponding part of the gradient. Discontinuities within the dataset were revealed by applying a Ward hierarchical clustering as an aggregation rule on Bray-Curtis dissimilarities with the *hclust* function of the stats package. Their significance was assessed by analysis of similarities (ANOSIM) based on Bray-Curtis dissimilarities and performed with the *anosim* function of the vegan package to infer statistical differences between groups when possible. Final clusters

were selected on the basis of the corresponding average silhouette width. The significance of the axis in each biplot representation was evaluated following Kaiser-Guttman criterion.

DR 1.10 Enumeration of total bacterial numbers

Microorganisms present in the environmental fluid were quantified by enumeration of total bacterial numbers by epifluorescence microscopy. 2 ml of sample were diluted into a 0.85% NaCl solution previously filtered to 0.2 µm in sterile conditions. 20 mL of the obtained solutions were filtered on a 0.2 µm sterile nitrocellulose filter mounted on a sterile PTFE filtration funnel device. Homogeneous repartition of the filtrate onto the filter was ensured by filling up the reservoir of the funnel prior to turning the vacuum on. 10 µL of 4',6-diamidino-2-phenylindole (DAPI) solution at 1 µg/mL were poured on each filter that were subsequently incubated in the dark at room temperature for 5 to 10 min. They were rinsed 3 times in a water bath, 3 times in a 80% ethanol bath and dried in the dark on a paper sheet for 10 to 15 min. Stained filters were mounted on a clean glass microscope slide with 10 µl of Citifluor anti-fading agent (Biovalley, Nanterre, France) and a glass cover slip. Samples were frozen and kept at -20°C until their observation.

DR 1.11 Characterization of fluid-bacteria interface by combined SEM and FIB-TEM approaches

At the end of each experiment, an aliquot of powder was recovered from each assay for electron microscopy observations. Samples were dried using the CO_2 critical point drying method. Briefly, water was first progressively replaced by ethanol by rinsing mineral powders with successive H_2O/ethanol solution containing an increasing proportion of ethanol (20%,

50%, 70%, 96%, 100%). Powders were recovered after each ~ 5 minute-long rinsing step on a filter (PC, ø = 0.22 µm) mounted on a Swinnex® filter holder set-up to avoid air-drying of the powder. Samples were then submitted to a standard critical point drying procedure consisting of 20 supercritical CO_2 cycles performed with a Leica EM CPD 300 apparatus.

Carbon-coated or gold-coated samples were observed with scanning electron microscopy (SEM) and energy dispersive X-ray (EDX) spectroscopy on a Tescan® VEGA II microscope. Some samples were re-coated with a thick carbon layer to prevent Pt and Ga ion beam damages to the sample (Lee et al., 2007) and ultrathin electron transparent cross sections were subsequently milled by focused ion beam (FIB) following conventional procedures (Saldi et al., 2015) through areas of interest covered with bacteria. Microbe-mineral interfaces were investigated on FIB thin sections by transmission electron microscopy (TEM) using a JEOL 2100F microscope operating at 200 kV in both TEM and STEM modes, equipped with an Energy Dispersive X-ray (EDX) detector.

DR 1.12 Thermodynamic Modeling

Saturation indices for labradorite, olivine and potential secondary phases were calculated using the Chess® software (Van der Lee and De Windt, 2002) and the Chess® tdb database (Lawrence Livermore National Laboratories EQ3/6 database, 8th version). To better reproduce the weak acidity induced by natural organic matter, measured pH was used as an input parameter. Dioxygen fugacity was set to 2 atm, matching the measured value of 4 to 8 ppm of dissolved dioxygen. The simulations did not indicate saturation with respect to any phase from the database likely to incorporate our tracers (i.e. Ca, Mg), aside from polymorphs of nontronite (nontronite-Mg, nontronite-Ca) or beidellite (beidellite-Mg, beidellite-Ca, see Table DR 2.4 and DR 2.5). However, the latter aluminosilicates were however unlikely to

precipitate under present experimental conditions (Yang and Steefel, 2008) and were not detected in the recovered samples by SEM.

REFERENCES

Daval, D., Sissmann, O., Menguy, N., Saldi, G. D., Guyot, F., Martinez, I., Corvisier, J., Garcia, B., Machouk, I., Knauss, K. G., and Hellmann, R., 2011, Influence of amorphous silica layer formation on the dissolution rate of olivine at 90°C and elevated pCO(2): Chemical Geology, v. 284, no. 1-2, p. 193-209.

Edgar, R. C., 2010, Search and clustering orders of magnitude faster than BLAST: Bioinformatics, v. 26, no. 19, p. 2460-2461.

Edgar, R. C., 2013, UPARSE: highly accurate OTU sequences from microbial amplicon reads: Nat Meth, v. 10, no. 10, p. 996-998.

Edgar, R. C., Haas, B. J., Clemente, J. C., Quince, C., and Knight, R., 2011, UCHIME improves sensitivity and speed of chimera detection: Bioinformatics, v. 27, no. 16, p. 2194-2200.

Lee, M. R., Brown, D. J., Smith, C. L., Hodson, M. E., Mackenzie, M., and Hellmann, R., 2007, Characterization of mineral surfaces using FIB and TEM: A case study of naturally weathered alkali feldspars: American Mineralogist, v. 92, no. 8-9, p. 1383-1394.

Saldi, G. D., Daval, D., Guo, H., Guyot, F., Bernard, S., Le Guillou, C., Davis, J. A., and Knauss, K. G., 2015, Mineralogical evolution of Fe–Si-rich layers at the olivine-water interface during carbonation reactions: American Mineralogist, v. 100, no. 11-12, p. 2655-2669.

Schloss, P., Westcott, S., Ryabin, T., Hall, J., Hartmann, M., Hollister, E., Lesniewski, R., Oakley, B., Parks, D., Robinson, C., Sahl, J., Stres, B., Thallinger, G., Van Horn, D., and Weber, C., 2009, Introducing mothur: Open-Source, Platform-Independent, Community-Supported Software for Describing and Comparing Microbial Communities: Applied and Environmental Microbiology, v. 75, no. 23, p. 7537-7541.

Van der Lee, J., and De Windt, L., 2002, CHESS Tutorial and Cookbook. Updated for version 3.0., Paris, 116 p.:

Walters, W. A., Caporaso, J. G., Lauber, C. L., Berg-Lyons, D., Fierer, N., and Knight, R., 2011, PrimerProspector: de novo design and taxonomic analysis of barcoded polymerase chain reaction primers: Bioinformatics, v. 27, no. 8, p. 1159-1161.

Wild, B., Daval, D., Guyot, F., Knauss, K. G., Pollet-Villard, M., and Imfeld, G., 2016, pH-dependent control of feldspar dissolution rate by altered surface layers: Chemical Geology, v. 442, p. 148-159.

Yang, L., and Steefel, C. I., 2008, Kaolinite dissolution and precipitation kinetics at 22 °C and pH 4: Geochimica et Cosmochimica Acta, v. 72, no. 1, p. 99-116.

ITEM DR 2. EXTENDED RESULTS

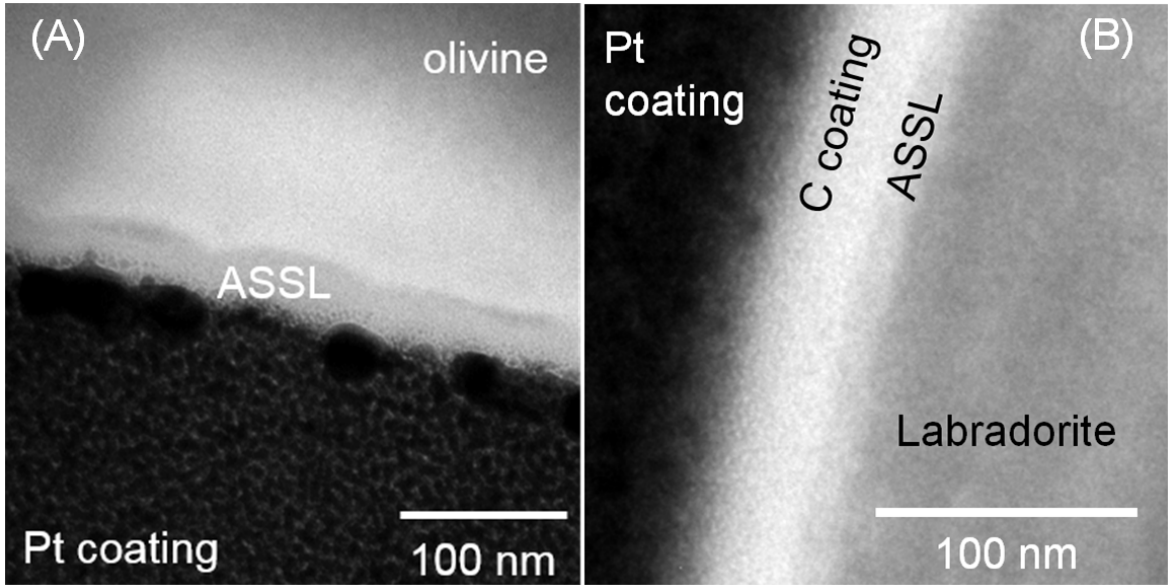

Figure DR2.1: Transmission electron microscope images representing olivine (A) and labradorite (B) passivation layers. Note that the physical and chemical characteristics of ASSLs developed at 80°C on labradorite and olivine in terms of thickness, chemical composition and atomic structural order are comparable to those developed on these minerals at lower temperatures (Johnson et al., 2014; Maher et al., 2016; Pokrovsky and Schott, 2000), and in the field over longer durations (Hellmann et al., 2012; Nugent et al., 1998). Of note and as mentioned in several studies (e.g., Gout *et al.*, 1997; Nugent *et al.*, 1998; Daval *et al.*, 2011, ASSLs are spatially discontinuous, and do not necessarily cover the whole surface of a dissolved crystals, explaining why we also observed some portions of weathered labradorite and olivine surface that were devoid of ASSLs.

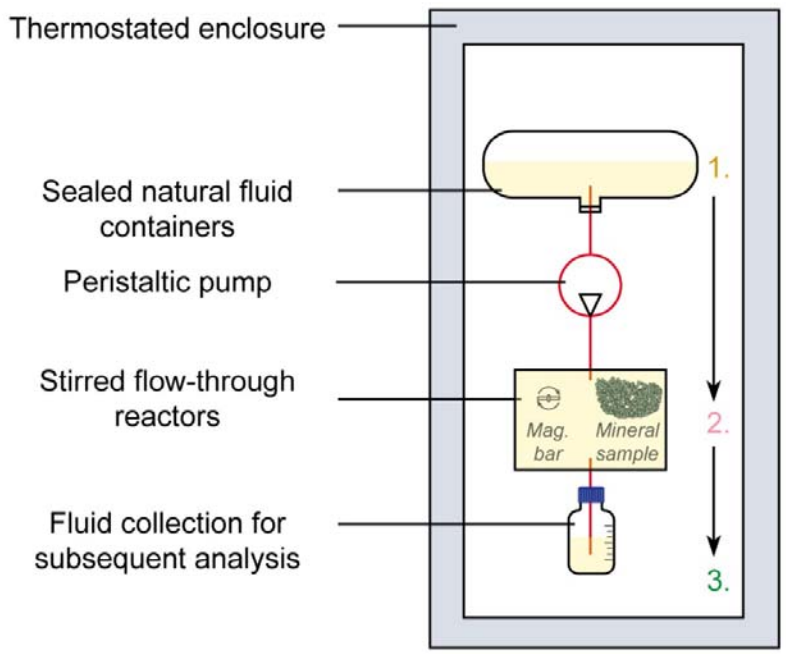

Figure DR2.2 : Schematic representation of the experimental setup used in this study. Soil solution stored in sealed containers (1.) is transferred to homogenized reactors (2.) by a peristaltic pump. Reacted fluid is continuously collected at the output of the flow-through system (3.) and analyzed.

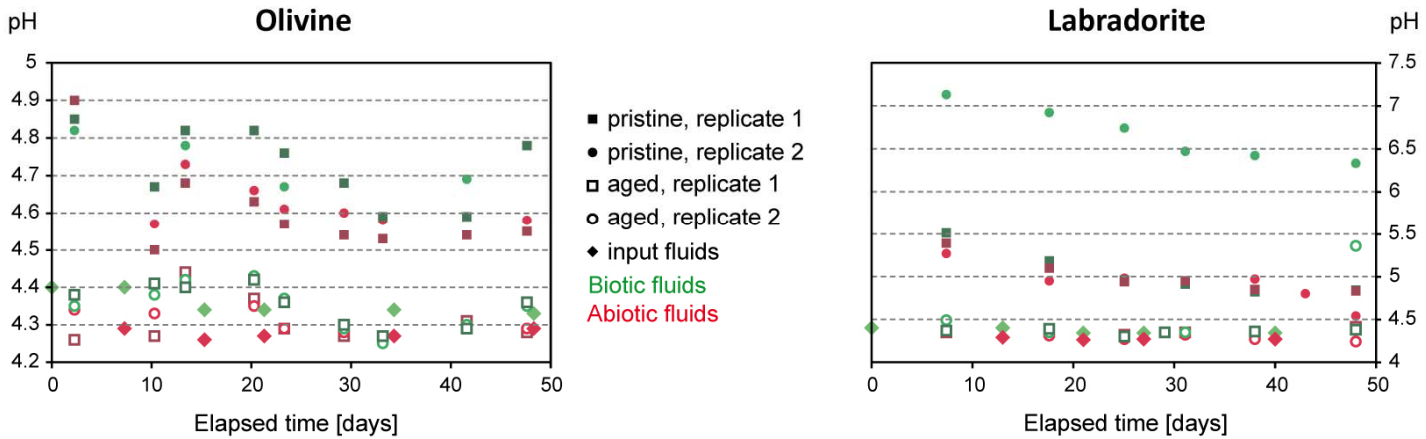

Figure DR2.3: Temporal evolution of pH for output (squares, circles) and input (diamonds) solutions. Open symbols correspond to experiments with aged minerals, either olivine, or labradorite.

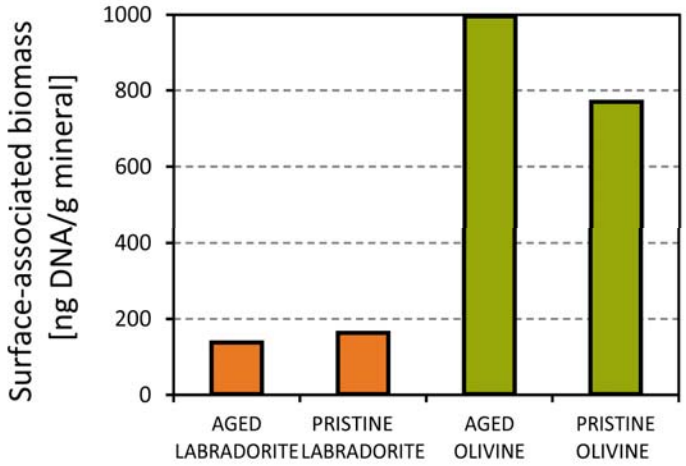

Figure DR2.4: Extractable DNA as a proxy for biomass associated with mineral substrates..

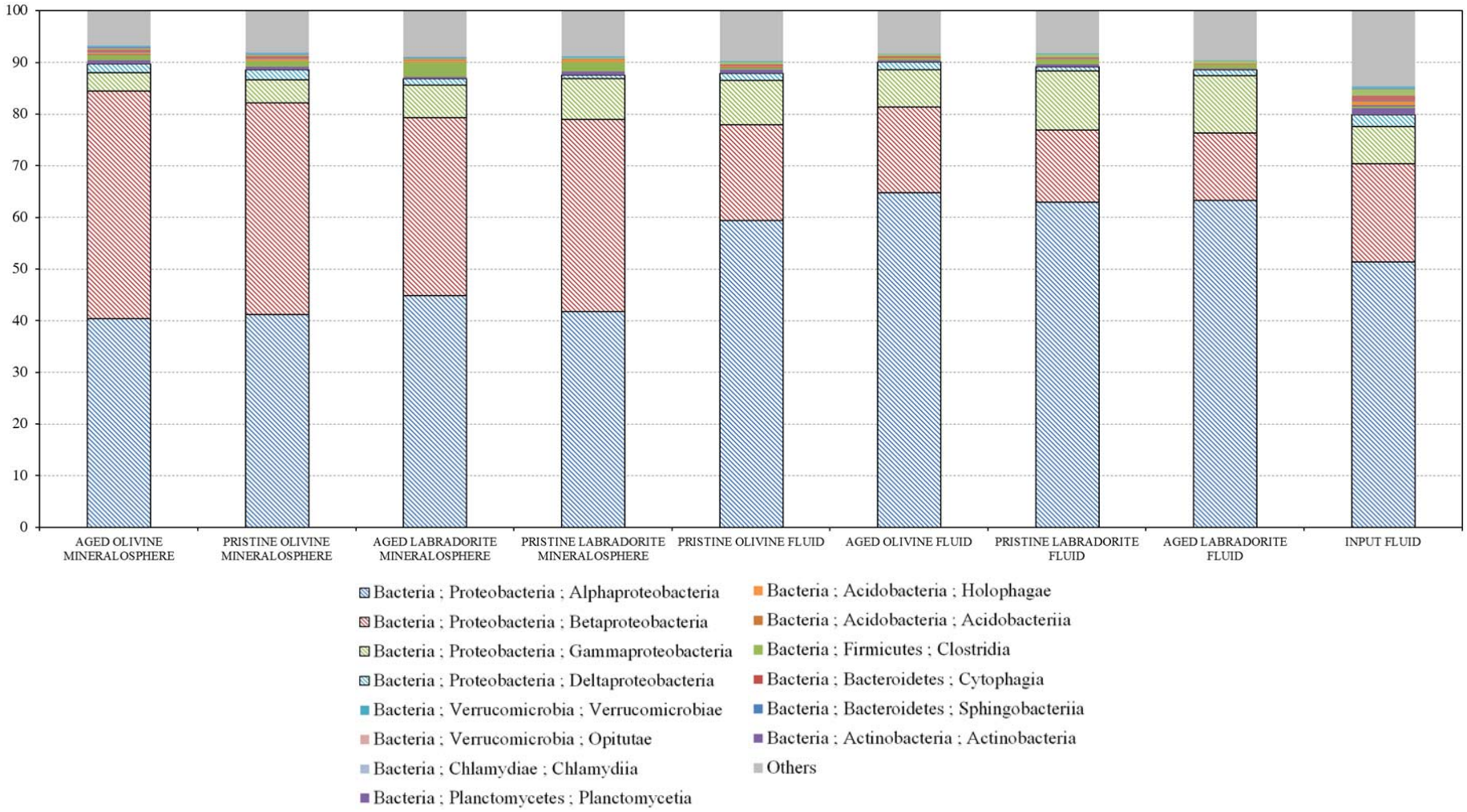

Figure DR2.5: relative abundance of the main bacterial taxa detected across the samples. Legend indicates "Kingdom ; Phylum ; Class". Striped bars correspond to different bacterial Classes belonging to Proteobacteria.

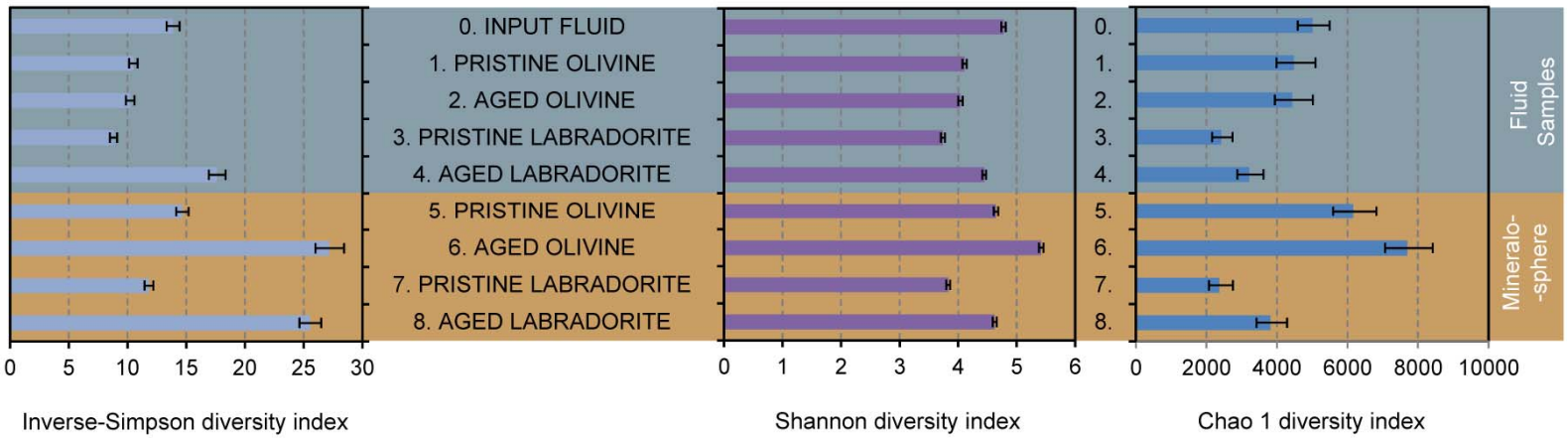

Figure DR2.6: α-diversity of bacterial communities obtained for both fluid and mineralosphere samples.

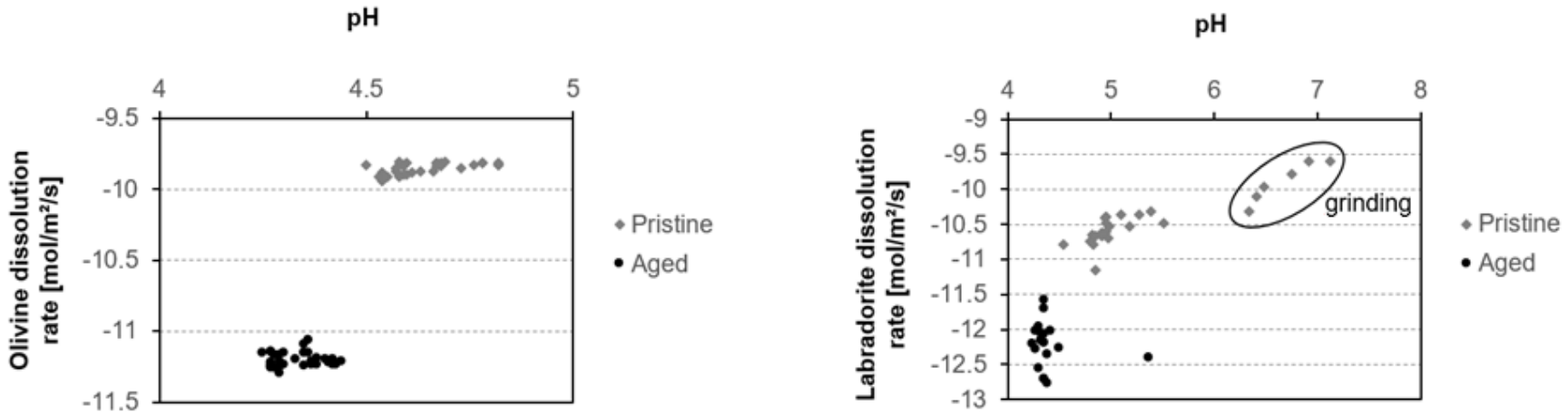

Figure DR2.7: Dissolution rates as a function of pH. Note that the main parameter controlling the dissolution rates is related to the physicochemical properties of the silicate surface (fresh or aged powders).

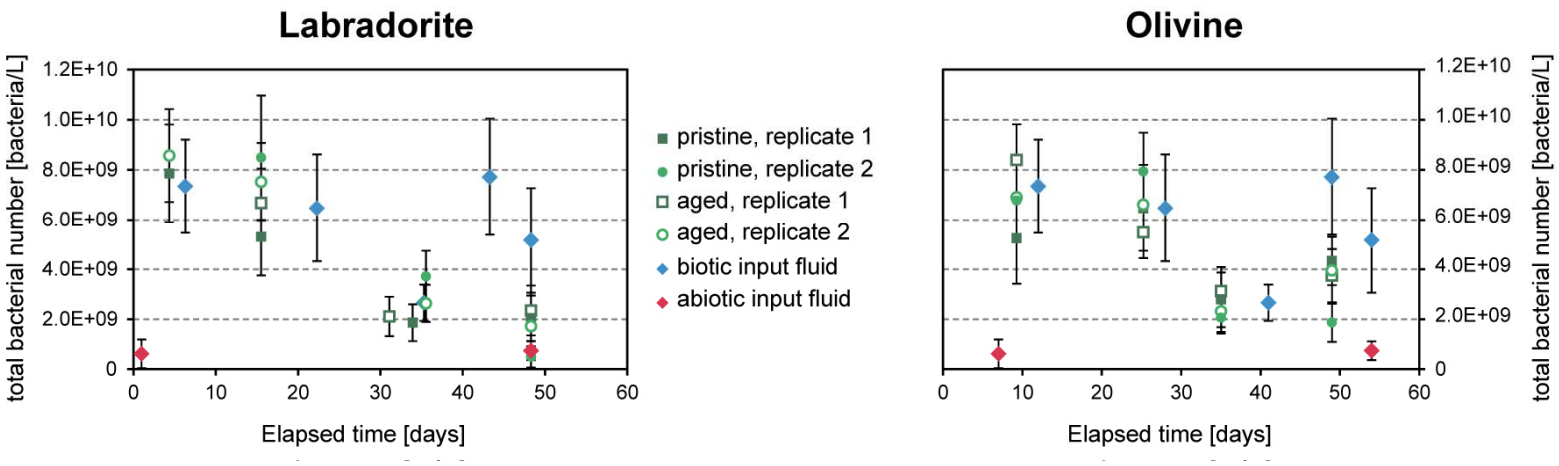

Figure DR2.8: Temporal evolution of bacterial concentrations as determined for output (squares, circles) and input (diamonds) solutions by epifluorescence microscopy (DAPI staining).

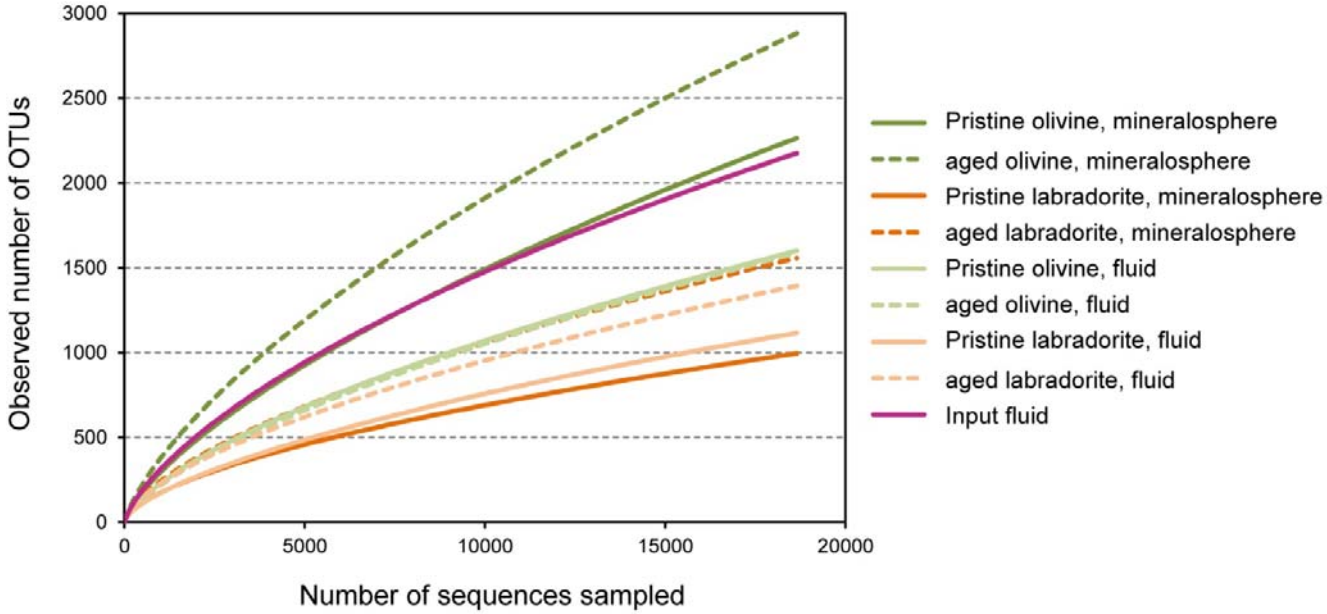

Figure DR2.9: Rarefaction curves for bacterial OTUs clustering at 97% sequence identity.

Pristine olivine, biotic fluid, replicate 1, m = 0.560 g, T = 12°C						
Si [ppm]	**Mg [ppm]**	**Fe [ppm]**	**time [days]**	**Flow rate [ml/min]**	**Rate (Mg) [mol/m²/s]**	**Rate (Si) [mol/m²/s]**
1.449	0.033	0.22	0	-	-	-
1.656	0.456	0.336	0.21	-	-	-
1.702	0.508	0.347	5.6	0.026	1.45E-10	7.78E-11
1.686	0.473	0.321	10.31	0.028	1.45E-10	8.66E-11
1.678	0.468	0.317	14.35	0.03	1.54E-10	9.86E-11
1.676	0.47	0.316	16.3	0.028	1.44E-10	9.56E-11
1.676	0.467	0.307	19.59	0.029	1.48E-10	1.07E-10
1.684	0.485	0.288	23.31	0.028	1.49E-10	1.20E-10
1.674	0.497	0.272	30.29	0.028	1.53E-10	1.15E-10
1.708	0.503	0.269	33.19	0.027	1.50E-10	1.28E-10
1.703	0.513	0.285	37.29	0.027	1.53E-10	1.25E-10
1.663	0.498	0.266	42.59	0.027	1.48E-10	1.06E-10
1.683	0.509	0.257	47.63	0.028	1.56E-10	1.20E-10
1.665	0.506	0.248	48.92	0.028	1.55E-10	1.11E-10
1.820**	0.724**	0.259**	49.5	0.028	-	-

Pristine olivine, biotic fluid, replicate 2, m = 0.542 g, T = 12°C						
Si [ppm]	**Mg [ppm]**	**Fe [ppm]**	**time [days]**	**Flow rate [ml/min]**	**Rate (Mg) [mol/m²/s]**	**Rate (Si) [mol/m²/s]**
1.449	0.033	0.22	0	-	-	-
*	*	*	0.21	-	-	-
1.728	0.51	0.348	5.6	0.029	1.68E-10	1.04E-10
1.748	0.48	0.338	10.31	0.028	1.52E-10	1.22E-10
1.724	0.472	0.324	14.35	0.029	1.55E-10	1.24E-10
1.748	0.481	0.326	16.3	0.028	1.53E-10	1.37E-10
1.719	0.474	0.318	19.59	0.028	1.50E-10	1.29E-10
1.747	0.496	0.304	23.31	0.027	1.52E-10	1.52E-10
1.715	0.502	0.263	30.29	0.027	1.54E-10	1.36E-10
1.752	0.519	0.273	33.19	0.027	1.60E-10	1.54E-10
1.734	0.52	0.289	37.29	0.027	1.60E-10	1.45E-10
1.69	0.513	0.268	42.59	0.027	1.58E-10	1.23E-10
1.709	0.531	0.247	47.63	-	-	-
1.742	0.577	0.255	48.92	-	-	-
1.843	0.712	0.239	49.5	-	-	-

Aged olivine, biotic fluid, replicate 1, m = 0.603 g, T = 12°C						
Si [ppm]	**Mg [ppm]**	**Fe [ppm]**	**time [days]**	**Flow rate [ml/min]**	**Rate (Mg) [mol/m²/s]**	**Rate (Si) [mol/m²/s]**
1.449	0.033	0.22	0	-	-	-
1.481	0.058	0.311	0.21	0.022	6.47E-12	NaN
1.494	0.05	0.313	5.6	0.028	5.80E-12	NaN
1.5	0.051	0.3	10.31	0.028	6.10E-12	NaN
1.491	0.051	0.279	14.35	0.029	6.32E-12	NaN

*	*	*	16.3	-	-	-
1.493	0.051	0.265	19.59	0.027	5.88E-12	8.65E-12
1.484	0.055	0.232	23.31	0.027	7.06E-12	1.60E-11
1.481	0.055	0.223	30.29	0.027	7.06E-12	1.47E-11
1.477	0.056	0.207	33.19	0.027	7.35E-12	1.28E-11
1.472	0.058	0.222	37.29	0.027	7.94E-12	1.05E-11
1.461	0.055	0.213	42.59	-	-	-
1.456	0.064	0.201	47.63	0.027	8.82E-12	3.21E-12
1.458	0.064	0.196	48.92	0.027	8.53E-12	4.12E-12
1.455**	0.081**	0.181**	49.5	0.027	-	-

Aged olivine, biotic fluid, replicate 2, m = 0.569 g, T = 12°C

Si [ppm]	Mg [ppm]	Fe [ppm]	time [days]	Flow rate [ml/min]	Rate (Mg) [mol/m²/s]	Rate (Si) [mol/m²/s]
1.449	0.033	0.22	0	-	-	-
1.457	0.054	0.305	0.21	0.027	7.17E-12	NaN
1.435	0.049	0.29	5.6	0.025	5.20E-12	NaN
1.479	0.049	0.289	10.31	0.028	5.82E-12	NaN
1.482	0.049	0.273	14.35	0.029	6.03E-12	NaN
1.495	0.049	0.271	16.3	0.028	5.82E-12	2.92E-12
1.461	0.049	0.26	19.59	0.028	5.82E-12	NaN
1.477	0.051	0.253	23.31	0.027	6.23E-12	1.36E-11
1.478	0.053	0.24	30.29	0.027	6.86E-12	1.41E-11
1.502	0.054	0.213	33.19	0.027	7.17E-12	2.57E-11
1.446	0.056	0.216	37.29	0.027	7.79E-12	NaN
1.414	0.054	0.209	42.59	-	-	-
1.434	0.059	0.201	47.63	0.028	8.08E-12	NaN
1.44	0.059	0.198	48.92	0.028	7.76E-12	NaN
1.460**	0.075**	0.185**	49.5	0.028	-	-

Pristine olivine, abiotic fluid, replicate 1, m = 0.562 g, T = 12°C

Si [ppm]	Mg [ppm]	Fe [ppm]	time [days]	Flow rate [ml/min]	Rate (Mg) [mol/m²/s]	Rate (Si) [mol/m²/s]
1.45	0.031	0.286	0	-	-	-
1.683	0.455	0.384	0.21	-	-	-
1.828	0.595	0.399	5.6	0.028	1.85E-10	1.33E-10
1.781	0.49	0.375	10.31	0.028	1.50E-10	1.26E-10
1.756	0.467	0.36	14.35	0.029	1.48E-10	1.33E-10
1.761	0.458	0.368	16.3	0.028	1.40E-10	1.38E-10
1.739	0.447	0.36	19.59	0.028	1.36E-10	1.38E-10
1.725	0.442	0.338	23.31	0.028	1.35E-10	1.40E-10
1.699	0.428	0.342	30.29	0.028	1.30E-10	1.27E-10
1.74	0.431	0.341	33.19	0.027	1.26E-10	1.42E-10
1.748	0.434	0.341	37.29	0.025	1.18E-10	1.36E-10
1.688	0.42	0.317	42.59	0.025	1.14E-10	1.08E-10
1.726	0.427	0.33	47.63	0.027	1.25E-10	1.36E-10
1.741	0.431	0.326	48.92	0.027	1.26E-10	1.43E-10

1.842**	0.586**	0.347**	49.5	0.027	-	-

Pristine olivine, abiotic fluid, replicate 2, m = 0.625 g, T = 12°C

Si [ppm]	Mg [ppm]	Fe [ppm]	time [days]	Flow rate [ml/min]	Rate (Mg) [mol/m²/s]	Rate (Si) [mol/m²/s]
1.45	0.031	0.286	0	-	-	-
1.716	0.495	0.399	0.21	-	-	-
1.822	0.63	0.399	5.6	0.028	1.76E-10	1.17E-10
1.778	0.534	0.363	10.31	0.027	1.43E-10	1.08E-10
1.773	0.518	0.369	14.35	0.028	1.43E-10	1.23E-10
1.748	0.504	0.356	16.3	0.028	1.39E-10	1.18E-10
1.747	0.494	0.365	19.59	0.028	1.36E-10	1.28E-10
1.743	0.49	0.337	23.31	0.027	1.30E-10	1.29E-10
1.752	0.485	0.343	30.29	0.027	1.29E-10	1.33E-10
1.74	0.485	0.337	33.19	0.027	1.29E-10	1.28E-10
1.755	0.494	0.342	37.29	0.027	1.31E-10	1.35E-10
1.726	0.487	0.323	42.59	0.027	1.29E-10	1.22E-10
1.732	0.476	0.321	47.63	0.027	1.26E-10	1.25E-10
1.775	0.493	0.324	48.92	0.027	1.31E-10	1.44E-10
1.912**	0.698**	0.359**	49.5	0.027	-	-

Aged olivine, abiotic fluid, replicate 1, m = 0.560 g, T = 12°C

Si [ppm]	Mg [ppm]	Fe [ppm]	time [days]	Flow rate [ml/min]	Rate (Mg) [mol/m²/s]	Rate (Si) [mol/m²/s]
1.45	0.031	0.286	0	-	-	-
1.472	0.069	0.339	0.21	-	-	-
1.54	0.054	0.343	5.6	-	-	-
1.545	0.053	0.325	10.31	0.028	7.23E-12	5.79E-12
1.539	0.05	0.316	14.35	0.028	6.24E-12	1.74E-11
1.534	0.05	0.323	16.3	0.027	6.02E-12	2.12E-11
1.505	0.049	0.308	19.59	0.028	5.91E-12	1.91E-11
1.499	0.048	0.295	23.31	0.026	5.19E-12	2.32E-11
1.532	0.051	0.298	30.29	0.026	6.10E-12	3.89E-11
1.548	0.052	0.306	33.19	0.023	5.67E-12	4.11E-11
1.559	0.066	0.305	37.29	-	-	-
1.522	0.069	0.29	42.59	-	-	-
1.501	0.052	0.285	47.63	0.028	6.90E-12	2.60E-11
1.511	0.052	0.282	48.92	0.028	6.90E-12	3.11E-11
1.517**	0.061**	0.270**	49.5	0.028	-	-

Aged olivine, abiotic fluid, replicate 2, m = 0.574 g, T = 12°C

Si [ppm]	Mg [ppm]	Fe [ppm]	time [days]	Flow rate [ml/min]	Rate (Mg) [mol/m²/s]	Rate (Si) [mol/m²/s]
1.45	0.031	0.286	0	-	-	-
1.376	0.052	0.333	0.21	-	-	-
1.511	0.05	0.326	5.6	0.029	6.31E-12	NaN
1.453	0.051	0.308	10.31	0.028	6.41E-12	NaN
1.521	0.05	0.321	14.35	0.029	6.31E-12	8.30E-12

1.564	0.051	0.325	16.3	0.028	6.41E-12	3.64E-11
1.51	0.049	0.315	19.59	0.028	5.77E-12	2.11E-11
1.522	0.049	0.298	23.31	0.027	5.56E-12	3.46E-11
1.525	0.049	0.299	30.29	0.027	5.56E-12	3.60E-11
1.516	0.049	0.295	33.19	0.027	5.56E-12	3.17E-11
1.523	0.051	0.308	37.29	0.027	6.18E-12	3.50E-11
1.465	0.051	0.276	42.59	0.026	5.95E-12	6.86E-12
1.502	0.051	0.275	47.63	0.027	6.18E-12	2.49E-11
1.495	0.051	0.273	48.92	0.027	6.18E-12	2.16E-11
1.435**	0.060**	0.250**	49.5	0.027	-	-

Input solutions							
Biotic input, measured		Biotic input		Abiotic input, measured		Abiotic input	
Mg [ppm]	time [days]	Mg [ppm]	time [days]	Mg [ppm]	time [days]	Mg [ppm]	time [days]
0.031	0	0.031	0.04	0.031	0	0.031	0.04
0.03	21.79	0.031	0.25	0.031	21.79	0.031	0.25
0.03	27.71	0.031	5.64	0.03	27.71	0.031	5.64
0.031	35.85	0.031	10.35	0.031	35.85	0.031	10.35
0.032	40.82	0.031	14.39	0.031	40.82	0.031	14.39
0.04	54.54	0.031	16.34	0.032	54.54	0.031	16.34
		0.031	19.63			0.031	19.63
		0.031	23.35			0.031	23.35
		0.031	31.21			0.031	31.21
		0.031	33.22			0.031	33.22
		0.031	37.33			0.031	37.33
		0.031	42.63			0.031	42.63
		0.034	47.67			0.031	47.67
		0.035	48.95			0.031	48.95
		0.035	49.54			0.031	49.54

Table DR2.1: Concentration data related to olivine experiments. - Unstable flow rate, could not be estimated; * no fluid collected due to insufficient flow rate; ** Polluted samples during tube changing; NaN Too close to background level to estimate the dissolution rate (ΔC<0).

Pristine labradorite, biotic fluid, replicate 1, m = 1.845 g, T = 12°C							
Si [ppm]	Al [ppm]	Ca [ppm]	Na [ppm]	time [days]	Flow rate [ml/min]	Rate (Ca) [mol/m²/s]	Rate (Si) [mol/m²/s]
1.449	0.591	0.058	0.891	0	-	-	-
1.404	0.561	0.958	0.867	1.04	0.004	2.97E-11	NaN
1.469	0.573	1.056	0.908	9.03	0.004	3.31E-11	NaN
1.414	0.573	0.952	0.847	16.57	0.004	2.98E-11	NaN
1.415	0.574	0.833	0.836	21.52	0.005	3.24E-11	NaN
1.433	0.588	0.689	0.848	31.11	0.004	2.13E-11	NaN
1.425	0.579	0.662	0.842	32.49	0.005	2.55E-11	NaN

1.44	0.588	0.639	0.856	33.94	0.003	1.47E-11	NaN
*	*	*	*	35.55	0	-	-
1.394	0.568	0.611	0.824	36.44	0.003	1.40E-11	NaN
1.405	0.581	0.583	0.844	37.42	0.005	2.22E-11	NaN
1.439	0.591	0.522	0.866	43.35	0.005	1.97E-11	NaN
1.408	0.564	0.474	0.839	47.3	0.002	7.08E-12	NaN

Pristine labradorite, biotic fluid, replicate 2, m = 1.863 g, T = 12°C

Si [ppm]	Al [ppm]	Ca [ppm]	Na [ppm]	time [days]	Flow rate [ml/min]	Rate (Ca) [mol/m²/s]	Rate (Si) [mol/m²/s]
1.449	0.591	0.058	0.891	0	-	-	-
1.428	0.474	4.935	0.914	1.04	0.003	1.22E-10	NaN
1.377	0.362	7.532	0.901	9.03	0.004	2.51E-10	NaN
1.387	0.393	6.146	0.878	16.57	0.005	2.55E-10	NaN
1.409	0.415	4.988	0.875	21.52	0.004	1.65E-10	NaN
1.432	0.467	3.228	0.907	31.11	0.004	1.07E-10	NaN
1.447	0.47	2.976	0.876	32.49	0.004	9.81E-11	NaN
1.435	0.479	2.357	0.864	33.94	0.004	7.73E-11	NaN
1.397	0.461	2.424	0.836	35.55	0.002	3.98E-11	NaN
1.388	0.464	2.493	0.819	36.44	0.004	8.19E-11	NaN
1.403	0.478	2.37	0.841	37.42	0.004	7.77E-11	NaN
1.424	0.503	1.859	0.831	43.35	0.004	6.06E-11	NaN
1.428	0.491	1.498	0.831	47.3	0.004	4.85E-11	NaN

Aged labradorite, biotic fluid, replicate 1, m = 1.835 g, T = 12°C

Si [ppm]	Al [ppm]	Ca [ppm]	Na [ppm]	time [days]	Flow rate [ml/min]	Rate (Ca) [mol/m²/s]	Rate (Si) [mol/m²/s]
1.449	0.591	0.058	0.891	0	-	-	-
1.441	0.587	0.108	0.96	1.04	0.006	1.18E-12	NaN
1.47	0.633	0.077	0.919	9.03	0.004	NaN	NaN
1.45	0.634	0.08	0.895	16.57	0.004	1.71E-13	NaN
1.448	0.631	0.069	0.877	21.52	0.004	NaN	NaN
1.447	0.625	0.086	0.869	31.11	0.002	3.93E-13	NaN
*	*	*	*	32.49	0	-	-
*	*	*	*	33.94	-	-	-
*	*	*	*	35.55	0	-	-
1.411	0.604	0.101	0.857	36.44	0	0.00E+00	0.00E+00
*	*	*	*	37.42	0	-	-
1.411	0.613	0.064	0.842	43.35	0.001	5.12E-14	NaN
1.432	0.575	0.07	0.861	47.3	0.004	4.44E-13	NaN

Aged labradorite, biotic fluid, replicate 2, m = 1.842 g, T = 12°C

Si [ppm]	Al [ppm]	Ca [ppm]	Na [ppm]	time [days]	Flow rate [ml/min]	Rate (Ca) [mol/m²/s]	Rate (Si) [mol/m²/s]
1.449	0.591	0.058	0.891	0	-	-	-
1.444	0.602	0.112	0.971	1.04	0.003	6.89E-13	NaN
1.505	0.663	0.097	0.951	9.03	0.004	5.45E-13	NaN
*	*	*	*	16.57	-	-	-

1.493	0.649	0.078	0.914	21.52	0.004	2.72E-13	1.46E-14
1.451	0.653	0.069	0.885	31.11	0.004	2.04E-13	NaN
1.494	0.658	0.069	0.889	32.49	0.004	2.38E-13	3.50E-13
1.498	0.678	0.07	0.909	33.94	0.004	3.06E-13	4.21E-13
1.458	0.658	0.072	0.894	35.55	0.003	2.81E-13	3.41E-14
1.441	0.647	0.08	0.881	36.44	0.004	6.81E-13	NaN
1.473	0.662	0.066	0.896	37.42	0.004	2.04E-13	2.27E-13
1.436	0.636	0.062	0.861	43.35	0.004	1.36E-13	NaN
1.451	0.59	0.069	0.889	47.3	0.004	4.08E-13	6.72E-14

Pristine labradorite, abiotic fluid, replicate 1, m = 1.850 g, T = 12°C

Si [ppm]	Al [ppm]	Ca [ppm]	Na [ppm]	time [days]	Flow rate [ml/min]	Rate (Ca) [mol/m²/s]	Rate (Si) [mol/m²/s]
1.45	0.634	0.074	1.13	0	-	-	-
1.481	0.578	0.845	1.154	1.04	0.003	1.92E-11	NaN
1.499	0.555	1.223	1.16	9.03	0.005	4.81E-11	NaN
1.538	0.594	1.127	1.158	16.57	0.005	4.42E-11	1.28E-14
1.526	0.599	0.98	1.148	21.52	0.005	3.80E-11	1.83E-13
1.499	0.609	0.809	1.129	31.11	0.004	2.48E-11	2.78E-13
1.499	0.618	0.773	1.122	32.49	0.004	2.36E-11	3.23E-13
1.513	0.637	0.762	1.142	33.94	0.004	2.32E-11	5.08E-13
1.522	0.628	0.736	1.143	35.55	0.004	2.24E-11	6.42E-13
1.526	0.624	0.729	1.152	36.44	0.004	2.21E-11	7.04E-13
1.505	0.633	0.697	1.128	37.42	0.004	2.10E-11	5.14E-13
1.505	0.632	0.616	1.134	43.35	0.004	1.84E-11	6.06E-13
1.519	0.618	0.559	1.162	47.3	0.004	1.64E-11	7.67E-13

Pristine labradorite, abiotic fluid, replicate 2, m = 1.872 g, T = 12°C

Si [ppm]	Al [ppm]	Ca [ppm]	Na [ppm]	time [days]	Flow rate [ml/min]	Rate (Ca) [mol/m²/s]	Rate (Si) [mol/m²/s]
1.45	0.634	0.074	1.13	0	-	-	-
1.459	0.586	0.847	1.168	1.04	0.005	3.17E-11	NaN
1.35	0.534	1.133	1.115	9.03	0.005	4.37E-11	NaN
1.521	0.576	1.083	1.153	16.57	0.005	4.18E-11	NaN
1.508	0.585	0.971	1.144	21.52	0.004	2.98E-11	NaN
1.506	0.595	0.803	1.132	31.11	0.004	2.43E-11	3.45E-13
1.538	0.595	0.788	1.162	32.49	0.004	2.38E-11	7.09E-13
1.564	0.624	0.788	1.184	33.94	0.004	2.38E-11	1.01E-12
1.518	0.612	0.731	1.131	35.55	0.004	2.19E-11	5.95E-13
1.509	0.6	0.716	1.129	36.44	0.004	2.14E-11	5.26E-13
1.496	0.601	0.694	1.123	37.42	0.004	2.07E-11	4.19E-13
1.513	0.617	0.626	1.138	43.35	0.004	1.85E-11	6.79E-13
1.515	0.604	0.57	1.147	47.3	0.004	1.66E-11	7.18E-13

Aged labradorite, abiotic fluid, replicate 1, m = 1.822 g, T = 12°C

Si [ppm]	Al [ppm]	Ca [ppm]	Na [ppm]	time [days]	Flow rate [ml/min]	Rate (Ca) [mol/m²/s]	Rate (Si) [mol/m²/s]
1.45	0.634	0.074	1.13	0	-	-	-

1.498	0.6	0.15	1.259	1.04	0.003	1.55E-12	NaN
1.534	0.651	0.151	1.232	9.03	0.005	2.71E-12	NaN
1.534	0.66	0.104	1.199	16.57	0.005	8.60E-13	NaN
1.521	0.654	0.098	1.176	21.52	0.005	6.88E-13	1.22E-13
1.536	0.658	0.097	1.171	31.11	0.004	6.54E-13	6.62E-13
1.571	0.659	0.097	1.217	32.49	0.005	8.60E-13	1.33E-12
1.583	0.676	0.097	1.214	33.94	0.004	6.88E-13	1.23E-12
1.526	0.658	0.093	1.172	35.55	0.005	7.31E-13	8.67E-13
1.516	0.657	0.096	1.158	36.44	0.005	8.60E-13	7.66E-13
1.538	0.667	0.091	1.167	37.42	0.005	6.45E-13	1.08E-12
1.552	0.67	0.095	1.184	43.35	0.004	7.23E-13	1.10E-12
1.547	0.629	0.102	1.19	47.3	0.004	9.63E-13	1.07E-12

Pristine labradorite, abiotic fluid, replicate 2, m = 1.859 g, T = 12°C

Si [ppm]	Al [ppm]	Ca [ppm]	Na [ppm]	time [days]	Flow rate [ml/min]	Rate (Ca) [mol/m²/s]	Rate (Si) [mol/m²/s]
1.45	0.634	0.074	1.13	0	-	-	-
1.501	0.667	0.15	1.278	1.04	0.003	1.52E-12	NaN
1.557	0.7	0.137	1.251	9.03	0.005	2.07E-12	NaN
1.563	0.693	0.11	1.214	16.57	0.005	1.10E-12	3.27E-13
1.563	0.68	0.105	1.205	21.52	0.005	9.70E-13	6.47E-13
1.541	0.647	0.104	1.181	31.11	0.004	8.77E-13	6.99E-13
1.519	0.665	0.094	1.159	32.49	0.004	5.73E-13	5.23E-13
1.584	0.685	0.104	1.215	33.94	0.004	9.10E-13	1.22E-12
1.52	0.603	0.1	1.16	35.55	0.004	8.09E-13	6.19E-13
1.506	0.629	0.113	1.142	36.44	0.005	1.56E-12	6.25E-13
1.535	0.648	0.092	1.171	37.42	0.004	5.40E-13	8.14E-13
1.538	0.641	0.091	1.174	43.35	0.004	5.73E-13	9.35E-13
1.509	0.611	0.092	1.151	47.3	0.004	6.07E-13	6.63E-13

Input solutions

Biotic input, measured		Biotic input		Abiotic input, measured		Abiotic input	
Ca [ppm]	time [days]	Ca [ppm]	time [days]	Ca [ppm]	time [days]	Ca [ppm]	time [days]
0.085	0	0.085	0	0.09	0	0.09	0
0.061	21.79	0.085	1.04	0.075	21.79	0.09	1.04
0.055	27.71	0.081	9.03	0.074	27.71	0.088	9.03
0.057	35.85	0.075	16.57	0.074	35.85	0.084	16.57
0.056	40.82	0.07	21.52	0.073	40.82	0.082	21.52
0.06	54.54	0.063	31.11	0.075	54.54	0.078	31.11
		0.062	32.49			0.077	32.49
		0.061	33.94			0.077	33.94
		0.061	35.55			0.076	35.55
		0.06	36.44			0.076	36.44
		0.06	37.42			0.076	37.42
		0.058	43.35			0.074	43.35
		0.057	47.3			0.074	47.3

Table DR2.2: Concentration data related to labradorite experiments. - Unstable flow rate, could not be estimated; * no fluid collected due to insufficient flow rate; NaN Too close to background level to estimate the dissolution rate (ΔSi<0).

	Si [ppm]	Mg [ppm]	Fe [ppm]	Al [ppm]	Ca [ppm]	Na [ppm]	time [days]
Abiotic	1.607	0.031	0.284	0.635	0.090	1.127	0
	1.452	0.031	0.314	0.647	0.075	1.137	21.79
	1.460	0.030	0.300	0.638	0.074	1.137	27.71
	1.451	0.031	0.287	0.631	0.074	1.125	35.85
	1.430	0.031	0.270	0.632	0.073	1.123	40.82
	1.458	0.032	0.261	0.623	0.075	1.128	54.54
Biotic	1.564	0.031	0.208	0.549	0.085	0.893	0
	1.464	0.030	0.245	0.600	0.061	0.891	21.79
	1.421	0.030	0.234	0.596	0.055	0.883	27.71
	1.430	0.031	0.222	0.597	0.057	0.875	35.85
	1.482	0.032	0.210	0.596	0.056	0.902	40.82
	1.448	0.040	0.187	0.566	0.060	0.907	54.54

Table DR2.3: Measured concentrations of input fluids

Phase	Saturation Index
mineral Nontronite-H	11.14
mineral Nontronite-Mg	11
mineral Nontronite-Ca	10.85
mineral Nontronite-Na	10.32
mineral Hematite	9.657
mineral Goethite	4.366
mineral Fe(OH)3	4.295
mineral Fe(OH)3-ws	4.295
colloid >HFO	3.257
mineral Kaolinite	3.177
mineral Diaspore	1.691
mineral Pyrophyllite	1.682
mineral Beidellite-H	1.643
mineral Beidellite-Mg	1.504
mineral Beidellite-Ca	1.355
mineral Boehmite	1.264
mineral Gibbsite	1.159
mineral Beidellite-Na	0.8204
colloid >Quartz	0.1303
mineral Quartz	0.1303

Table DR 2.4: Chess output for a simulation corresponding to a theoretical solution where each cation concentration and the pH are set to their respective maximum value measured over the whole olivine dataset.

Phase	Saturation Index
mineral Nontronite-Ca	12.25
mineral Nontronite-H	12.19
mineral Nontronite-Mg	12.19
mineral Nontronite-Na	11.59
mineral Hematite	10.89
mineral Goethite	4.983
mineral Fe(OH)3-ws	4.912
mineral Fe(OH)3	4.912
colloid >HFO	3.874
mineral Kaolinite	3.749
mineral Beidellite-Ca	2.25
mineral Beidellite-H	2.199
mineral Beidellite-Mg	2.194
mineral Pyrophyllite	2.09
mineral Diaspore	2.058

mineral Boehmite	1.632
mineral Beidellite-Na	1.591
mineral Gibbsite	1.527
colloid >Quartz	0.04849
mineral Quartz	0.04849

Table DR 2.5: Chess output for a simulation corresponding to a theoretical solution where each cation concentration and the pH are set to their respective maximum value measured over the whole labradorite dataset.

REFERENCES

Daval, D., Sissmann, O., Menguy, N., Saldi, G. D., Guyot, F., Martinez, I., Corvisier, J., Garcia, B., Machouk, I., Knauss, K. G., and Hellmann, R., 2011, Influence of amorphous silica layer formation on the dissolution rate of olivine at 90°C and elevated pCO(2): Chemical Geology, v. 284, no. 1-2, p. 193-209.

Gout, R., Oelkers, E. H., Schott, J., and Zwick, A., 1997, The surface chemistry and structure of acid-leached albite: New insights on the dissolution mechanism of the alkali feldspars: Geochimica et Cosmochimica Acta, v. 61, no. 14, p. 3013-3018.

Hellmann, R., Wirth, R., Daval, D., Barnes, J.-P., Penisson, J.-M., Tisserand, D., Epicier, T., Florin, B., and Hervig, R. L., 2012, Unifying natural and laboratory chemical weathering with interfacial dissolution–reprecipitation: A study based on the nanometer-scale chemistry of fluid–silicate interfaces: Chemical Geology, v. 294–295, no. 0, p. 203-216.

Johnson, N. C., Thomas, B., Maher, K., Rosenbauer, R. J., Bird, D., and Brown Jr, G. E., 2014, Olivine dissolution and carbonation under conditions relevant for in situ carbon storage: Chemical Geology, v. 373, no. 0, p. 93-105.

Maher, K., Johnson, N. C., Jackson, A., Lammers, L. N., Torchinsky, A. B., Weaver, K. L., Bird, D. K., and Brown Jr, G. E., 2016, A spatially resolved surface kinetic model for forsterite dissolution: Geochimica et Cosmochimica Acta, v. 174, p. 313-334.

Nugent, M. A., Brantley, S. L., Pantano, C. G., and Maurice, P. A., 1998, The influence of natural mineral coatings on feldspar weathering: Nature, v. 395, no. 6702, p. 588-591.

Pokrovsky, O. S., and Schott, J., 2000, Forsterite surface composition in aqueous solutions: A combined potentiometric, electrokinetic, and spectroscopic approach: Geochimica et Cosmochimica Acta, v. 64, no. 19, p. 3299-3312.